Carbon 155 (2019) 462–468

Contents lists available at ScienceDirect

Carbon

journal homepage: www.elsevier.com/locate/carbon

Rapid roll-to-roll production of graphene films using intensive Joule heating

Yingjun Liu, Peng Li, Fang Wang, Wenzhang Fang, Zhen Xu*, Weiwei Gao, Chao Gao**

MOE Key Laboratory of Macromolecular Synthesis and Functionalization, Department of Polymer Science and Engineering, Key Laboratory of Adsorption and Separation Materials & Technologies of Zhejiang Province, Zhejiang University, 38 Zheda Road, Hangzhou, 310027, China

ARTICLE INFO

Article history:
Received 29 June 2019
Received in revised form
23 August 2019
Accepted 6 September 2019
Available online 6 September 2019

ABSTRACT

The development of rapid and scalable techniques for thermally conductive film is useful for the improved function and efficiency of electronic devices. The commercially available carbon film that made from polyimide film by sequential carbonization and graphitization in electrical furnace is usually produced in an intermittent way, which inevitably decreases the manufacturing efficiency and increases energy consumption and production cost. Macroscopic graphene film is considered to be an ideal alternative of traditional carbon film due to its combined merits of high thermal conductivity and flexibility. Here, we report a rapid approach to continuously fabricate graphene film by Joule heating of chemically reduced graphene oxide film integrated with a high-throughput roll-to-roll process. The achieved graphene film holds excellent electrical of 4.2×10^5 S/m and thermal conductivity of 1285 ± 20 W/mK. Moreover, the intensive Joule heating in a roll-to-roll manner is more time-saving, energy-efficient, and cost-effective than traditional heating method by electrical furnace. Such facial processing strategy offers new opportunities for the scaled-up manufacturing of large area graphene film with potential applications in the fields of thermal management, flexible electronics, and wearable devices.

1. Introduction

Rapidly increasing heat flux density in miniaturized electronic devices with intensive integrated circuits has posed significant challenges on thermal management materials [1–4]. Efficient dissipating the heat loads is becoming a critical issue for maintaining the reliability and extending fatigue life of high-power electronic system. Thermal conductive thin films with large heat-dissipation capability are urgently needed in high effective thermal management [5]. In response to these needs, copper and aluminum foils have been used as the main thermal management materials while they usually suffer from chemical oxidation/corrosion, heavy weight and limited thermal conductivity (400 W/mK). The commercially available carbon film that made from polyimide film by sequential carbonization and graphitization holds high in-plane thermal conductivity (up to 1750 W/mK), enabling it to serve as qualified heat spreading materials in modern microelectronic and optoelectronic applications. However, the severe demand on the molecular structure of original polyimide and the tedious time-consuming production procedure (including polymerization, film-forming, film-processing, long time carbonization and graphitization, etc.) seriously decrease the product yield rate and the manufacturing efficiency as well [6–8]. Moreover, another insuperable problem is the huge energy consumption when using traditional graphitization furnace to prepare highly thermally conductive carbon films.

Achieving advanced thermal management materials with optimal performance requires scalable and cost-effective fabrication approaches that incorporate novel chemicals, synthetic route, and methodology. Graphene, an atomically thin sheet of carbon atoms arranged in a 2D hexagonal lattice, offers great potential for next-generation thermal management [9–14]. Macroscopic graphene film (GF) assembled from graphene sheets are expected to be an ideal heat-dissipation material for high-powered devices due to its combined merits of high thermal conductivity and flexibility. For example, Xin et al. firstly reported a flexible GF with thermal conductivity of 1434 W/mK [15]. By choosing debris-free giant graphene sheets as basic building blocks, Peng et al. improved the

* Corresponding author.
** Corresponding author.
E-mail addresses: zhenxu@zju.edu.cn (Z. Xu), chaogao@zju.edu.cn (C. Gao).

https://doi.org/10.1016/j.carbon.2019.09.021
0008-6223/

thermal conductivity up to 1940 W/mK. Recently, Liu et al. prepared ultrathin GF with a record high thermal conductivity of 3200 W/mK by tailoring the sheet alignment and interlayer binding energy [16].

In pursuit of highly thermally conductive GF, high temperature annealing in an electrical furnace is indispensable for eliminating the oxygen-containing groups and restoring the structural defects [15,17,18]. It usually takes at least two days to complete the annealing process due to the retarded heating/cooling rate limited by the furnace itself [19,20]. Recently, several studies have demonstrated that electrical current induced Joule heating can substantially restore the conjugated skeleton in defective graphene blocks and dramatically improve the conductivity and carrier mobility of GF in a very short period [21–28]. The microstructure and sheet alignment can be finely controlled by adjusting the electrical current applied to the sample. However, the motionless electrode configuration and limited sample size with centimeter scale are not compatible with large-scale fabrication [21,29,30]. Therefore, continuously manufacturing free-standing highly conductive GF in a rapid and scalable manner remains challenging.

Here, we report a continuous, high-throughput, and energy-effective strategy for annealing GF *via* intensive Joule heating in a roll-to-roll manner. The input electrical power is directly exerted on the GF sample through rotated graphite rollers. As most of the applied power converts into heat energy of the film, the energy usage ratio should be much higher than traditional thermal treatment by electrical furnace. The achieved GF exhibits excellent thermal conductivity (1285 ± 20 W/mK) and electrical conductivity (4.2×10^5 S/m), both of which are comparable to that of GF annealed by furnace at the same temperature.

2. Experimental

2.1. Material preparation

Aqueous dispersion GO sheets with large lateral size of 15–20 μm (Fig. S1) was purchased from Hangzhou Gaoxi Technology Co. Ltd. The GO dispersion was coated on flat glass substrate by blade coating method to obtain GO film with controlled length, width, and thickness. The GO film was carefully peeled off from the substrate and chemically reduced by hydroiodic acid at 90 °C to get rGO film. Then the rGO film was repeatedly rinsed with large amount of ethanol to remove residual iodine and dried at 60 °C. The dried rGO film was further thermally reduced at 300 °C under mechanical pressure in H2/Ar (5%/95%) atmosphere to increase the electrical conductivity by remove most of oxygen-containing groups.

The Joule heating process was conducted in an argon-filled glovebox with water/oxygen content lower than 1 ppm. The rGO film was cut into strip with width of 1.5 cm for continuous Joule heating. The rGO film continuously passed through the rotating graphite rollers driven by two controllable micromotors at a speed of 0.1 m/min. The distance between the horizontally aligned graphite rollers can be tuned from 1 cm to 10 cm according to the resistance of the sample and the power supply capability of the source. An auto range DC power source (ITECH IT6522D) was used to supply programmed bias voltage across the graphite rollers by two electric brushes, causing a direct current flowing through the sample. We developed a two-step Joule heating reduction of rGO film to achieve GF. In the first step, the voltage increased at a slow ramp of 20 mV/s until the temperature of the film reached to ~1200 °C. In the second step, the film was further Joule heated to ~2400 °C under constant voltage (50 V) model. The total heating process takes about 20 min.

2.2. Material characterization

XPS measurement was performed on a photoelectron spectrometer (ESCALAB 250, ThermoFisher Scientific) with Al Kα as X-ray source. XRD was measured on an X'Pert PRO diffractometer (PANalytical) using Cu Kα1 radiation with an X-ray wavelength of 1.5406 Å. Raman spectroscopy and mapping scanning were recorded by a commercial Renishaw inVia-Reflex Raman microscope at an excitation wavelength of 532 nm. The morphology of the samples was taken on a field emission SEM (Hitachi S4800) at 10 kV. The temperature was monitored by fiber optic spectrometer (FX 2000) and two commercial noncontact two-color pyrometers (Fluke Endurances series E2RL-F1-L-0-0 for 250–1200 °C and Raytek Marathon MR1SC for 1000–3000 °C). The distance between the sample and the optical fiber was 35 cm. The electrical conductivity was tested using a four-probe method. Mechanical performance was tested on a universal testing machine (Instron 2344, USA) with a gauge length of 10 mm and a constant loading rate of 1.0 mm/min. Synchronous SAXS test was carried out in BL16B1 beam line station of Shanghai Synchrotron Radiation Facility (SSRF) with incident beam parallel to the film plane. The distance between sample and dector CCD was 1735 mm. Thermal conductivity was evaluated by a steady-state electrical heating method in a vacuum chamber. A Keithley 2460 source meter was used to supply electrical power. The temperature profile was recorded by a high resolution infrared imager (FLIR T630sc).

3. Results and discussion

To realize continuous reduction of GF by Joule heating, we delicately designed a roll-to-roll preparation system consisting of three parts: film-supplying, current-feeding and film-collecting, as illustrated in Fig. 1a. The chemically reduced graphene oxide film (rGO film) continuously passed through the rotating graphite rollers driven by two controllable micromotors (Fig. 1b, Video S1). A programmed voltage was applied across the parallel graphite rollers by two electric brushes and a direct current (DC) flows through rGO film, causing a temperature rise due to Joule heating effect. By tailoring the rotation speed of the rollers, the film could accommodate the size shrinking induced by the Joule heating treatment. The graphite rollers not only serve as rotating electrode, but also exert mechanical pressure on the Joule heated rGO film to obtain pure GF with condense structure.

Supplementary video related to this article can be found at https://doi.org/10.1016/j.carbon.2019.09.021.

The sequence snapshots in Fig. 1c show that the light intensity emitted from the film increases with the input power, indicating gradually increased temperature induced by the Joule heating. During the programmed heating process, we collected the emission spectra from 350 nm to 950 nm by a fiber optic spectrometer (Ideaoptics FX 2000) (Fig. 1d). Then the temperature of the film was extracted by fitting the spectra to a gray body radiation equation,

$$B_\lambda(\lambda, T) = \gamma\varepsilon \frac{2hc^2}{\lambda^5} \frac{1}{e^{hc/\lambda k_B T} - 1},$$

where γ is a scaling constant for fitting, ε is the emissivity, h is the Planck constant, c is the light speed, k_B is the Boltzmann constant, and λ is the wavelength [31–33]. Additionally, we also continuously recorded the temperature of the sample in real time by two commercial noncontact two-color pyrometers to ensure accuracy of the measurement. The temperature versus applied electrical power for the rGO film is shown in Fig. S2. The sublinear curve indicates the decrease of heating efficiency at higher temperature zone because more heat is dissipated by conduction and radiation at high

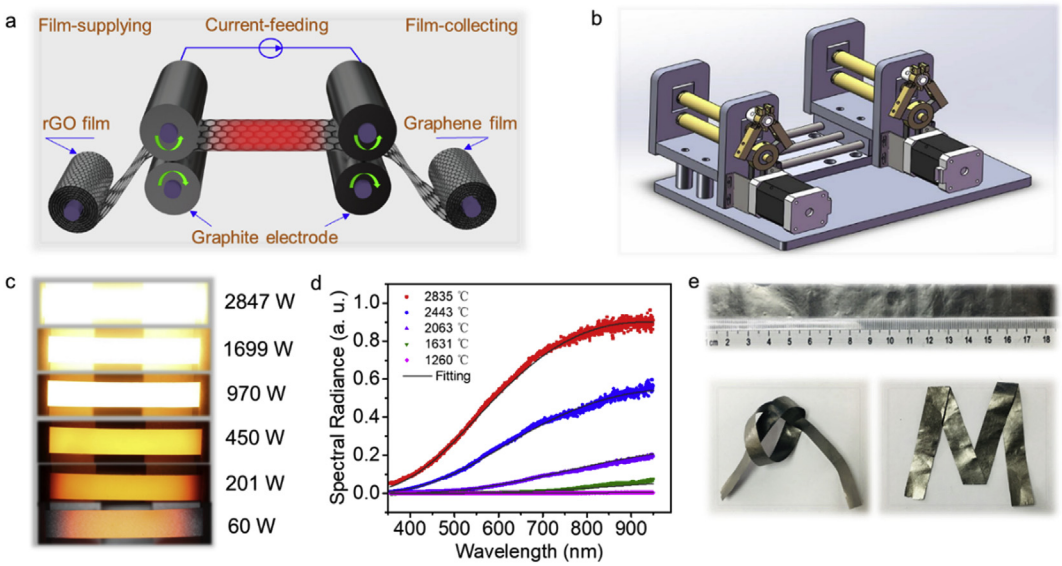

Fig. 1. (a) Schematic of the pressurized roll-based production of GFs by Joule heating. (b) Schematic of the continuous electrical-heating equipment driven by two speed-controllable motors. (c) Snapshots of the film heated by increasing electrical power from bottom to up. (d) Spectral radiance measurement of the film for different electrical power inputs. The temperature can be obtained by fitting the spectra to Planck's law. (e) Photos of the Joule-heated GF, exhibiting excellent flexibility and foldability. (A colour version of this figure can be viewed online.)

temperatures. Note that the temperature of the Joule heated film can reach as high as 2835 °C, while considering the safety and stability of our roll-to-roll equipment, the highest temperature was set as 2433 °C in real Joule heating process. Thereafter, the GF refers to the film Joule heated at 2433 °C unless otherwise stated.

We adopted a two-step Joule heating reduction to obtain high quality GF (Fig. S3a). In the first step, the voltage increased at a ramp of 20 mV/s. The slowly loading mode of voltage avoids the abrupt temperature rise that can cause unfavorable pores on the film due to the violent release of gas (Fig. S4). In the second step, higher temperature (~2400 °C) was achieved under constant voltage condition. Fig. S3b shows the typical *I-V* curve for the electrified sample with size of 1.5 cm × 6 cm. The current increased slowly with the applied voltage on the rGO film. When the voltage was increased to ~36 V, the current rapidly increased from 6 to 43 A. The significant increase in the conductivity is due to the removal of defects and impurities in rGO film during the high temperature treatment. By carefully tailoring the applied voltage, the velocity of the horizontally aligned graphite rollers, as well as the pressure (interspace) between the vertically aligned rollers, a continuous GF with width of 1.5 cm and length of 20 cm can be achieved within 20 min. Note that the maximum width of the processed rGO was limited by the width of the graphitic rollers and the power of the source in our experimental setup. The upper limit of the current that the DC power source (ITECH IT6522D) can be supplied is about 120 A. Therefore, the maximum width of film can be Joule heated using our experimental setup is about 4 cm. We envision that GF with much larger lateral dimension could be easily achieved by just increasing the width of the rollers and upgrading the power supply device.

The surface morphology of GF is featured with numerous protuberant wrinkles and ripples, as shown in Fig. 2a–c. The wrinkles and ripples originate from the microgasbags generated during the Joule heating process [17]. The cross-sectional images show well aligned multilayer stacking of graphene sheets. Such close contact between aligned graphene layers contributes to the transfer of phonon and electron, thereby facilitating the thermal and electrical conductive performance [34]. The order parameter of the continuously prepared GF with compacted structure (86.9%) is much higher than that of loosely stacked GF without continuous rolling compaction (75.3%, Fig. S5), as evidenced from the small-angle X-ray scattering (SAXS) patterns (Fig. 2g and h) and corresponding FWHM of the azimuthal scan curve (Fig. 2i). The compacted structure and better alignment of graphene sheets endows the GF with tensile strength of 16.7 MPa and Young's modulus of 0.32 GPa, both of which are higher than that of uncompacted GF (Fig. 2j).

We investigated the structural evolution of rGO film after Joule annealing by X-ray photoelectron spectroscopy (XPS), X-ray diffraction (XRD), and Raman spectroscopy, respectively. The carbon to oxygen (C/O) atomic ratio of rGO film treated at 1260 °C and 2443 °C are 15.3 and 50.4, respectively, which are much lower than that of initial rGO film, confirming the effective removal of the functional groups during the Joule heating reduction (Fig. 3a). The C1s spectra shown in Fig. 3b also give the same conclusion. The XRD pattern of rGO film shows a (002) reflection peak at 24.16° with a full width at half maximum (FWHM) of 2.02° (Fig. 3c). After high temperature reduction by Joule heating, the characteristic peak becomes much more sharp and narrow, with FWHM decreases to 0.784 for 1260 °C reduction and 0.22 for 2443 °C reduction. The narrow peak reveals the existence of uniform crystalline structure in annealed GF. The characteristic peak shifts from 24.19° to 26.48° after Joule heating at 2443 °C, corresponding to an interlayer distance reduced from 0.41 nm to 0.34 nm. The decreasing interspace distance is due to the effective removal of the functional groups in RGO film, which is consistent with the decline of oxygen containing groups as illustrated in XPS spectra (Fig. 3a and b). The crystallite size (Lc) in GF was estimated to be 37.13 nm using Scherrer equation, $Lc = 0.9\lambda/(\beta\cos\theta)$, where λ is the X-ray wavelength and β is FWHM of the (002) peak [35]. The large crystalline domains contribute to the high electrical and thermal conductivity of GF [36–38].

In Raman spectra (Fig. 3d), compared to the rGO film, the D band (1350 cm^{-1}) corresponding to defective carbon sites is suppressed tremendously and the G band associated with crystalline carbon (1585 cm^{-1}) remains as prominent peak with high intensity for the

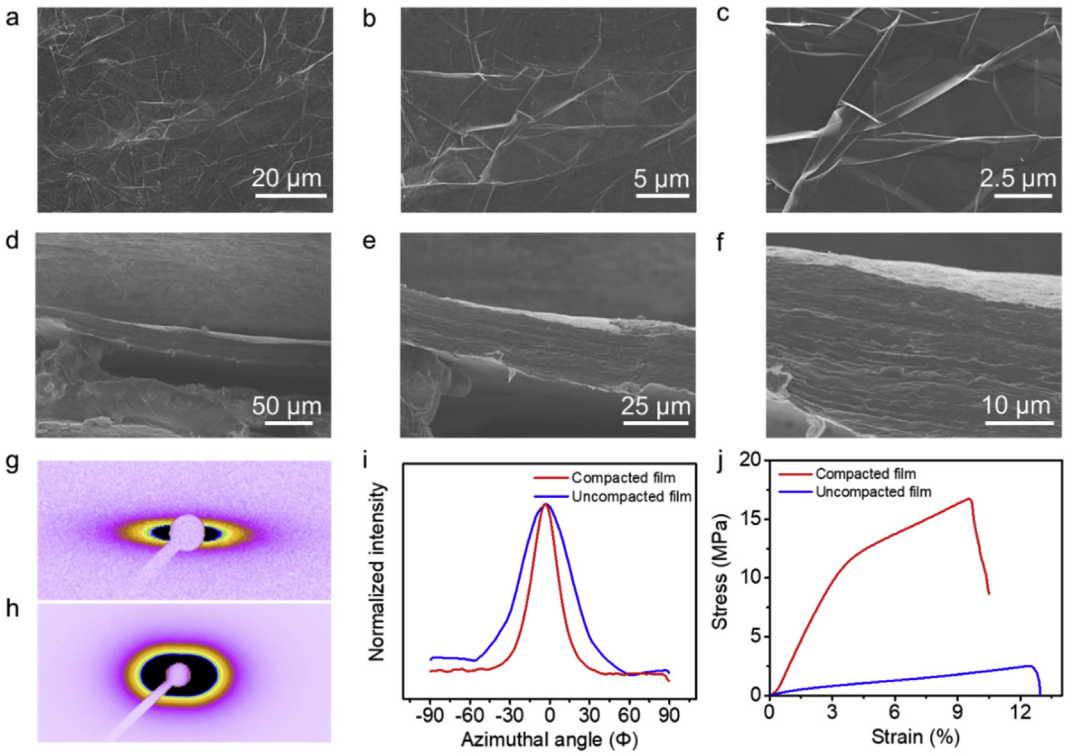

Fig. 2. (a-c) SEM images of the Joule heated GF with different magnifications, showing wrinkles and ripples on the surface. (d-f) Cross-sectional morphology of the Joule heated GF. (g-i) SAXS pattern of the compacted (g) and uncompacted (h) GF and corresponding azimuthal scan curve (i). The narrower FWHM of compacted GF signifies higher degree of orientation. (j) The stress-strain curves of the GF with different compacting states. (A colour version of this figure can be viewed online.)

film heated at 2443 °C. As a result, the intensity ratio (I_D/I_G) of the D peak and G peak decreases from 1.10 to 0.08, suggesting an effective recovery of structural defects by Joule heating [39]. Additionally, a sharp 2D band at 2720 cm^{-1} appears with an I_{2D}/I_G ratio of 0.97, which is closer to that of perfect single layer graphene, further confirming the highly crystalline structure of the GF after high temperature Joule annealing [40,41]. The symmetric 2D band can be fitted into a single Lorentzian peak, suggesting the presence of turbostratic stacking graphene [20,29,34].

To evaluate the uniformity of the Joule heated GF, we collected Raman spectra at different sites along the length direction of the film (Fig. 3e). The distance of each collecting site was about 1 cm. All the Raman data are similar, indicating the high uniformity of the GF in a long range. Additionally, we measured the resistance of the GF as a function of testing length. The resistance increases linearly with the testing length (Fig. 3f), further testifying structural homogeneous on large area. The Raman mapping images (Fig. S6 and Fig. 3g–i) of normalized intensity of D peak, G peak, and I_D/I_G demonstrate that the Joule heated GF is uniform in micron scale.

The thermal conductivity of GF at room temperature was measured by an optimized steady-state electrical heating method in a vacuum chamber (Fig. S7) [15,19,37]. In contrast to most studies where two electrodes are frequently used, here the GF was suspended between four copper blocks (Fig. 4a) which simultaneously served as heat sinks and electrodes. A Keithley 2460 source meter was used to supply direct current and to measure the voltage drop across the middle two electrodes by a standard four-wire method. This modified steady-state electrical heating method eliminates contact resistance, enabling much more reliable testing results about electrical conductivity and thermal conductivity thereof. When a direct current flows through the GF, the temperature will increase due to Joule heating effect. The temperature profile along GF was recorded by an infrared imager (FLIR T630sc) with a temperature resolution of 0.1 K in real time. When the temperature rise is not large (below 15 °C in this study), the radiative heat loss can be neglected. Then, we calculated the thermal conductivity (K) of conductive materials by the following equation that derives from one-dimensional steady-state heat transfer model,

$$K = \frac{UIL}{A_c(T_m - T_e)},$$

where U is the measured voltage across the middle two contacts, I is the applied direct current, L is the half-length between the middle two contacts, Ac is the cross cross-section area of the sample, and T_m and T_e are the temperature at the middle and end points of the suspended film, respectively. A thin layer of amorphous graphite was spray-coated on the GF sample and copper electrodes to ensure a uniform infrared emissivity before thermal conductivity measurement, which is critical to get accurate temperature profile by infrared imager (Fig. S8). Additionally, to maximize experimental accuracy, a series of temperature profiles were recorded at various applied powers (UI).

Fig. 4b shows the temperature profiles along the GF at different input power. The temperature profile obviously resembles a parabolic curve with the highest temperature presented in the middle point of the film, matching the one-dimensional steady-state heat transfer model. The relation between the temperature rise of the middle point and the input power is shown in Fig. 4c. The T_m-T_e is linear to the input power, ensuring the accuracy of the thermal conductivity measurement.

The thermal conductivity was obtained *via* the slope from the linear fitting T_m-T_e and UI. The calculated thermal conductivity of the GF reaches to 1285 ± 20 W/mK with a measurement uncertainty error of 10.4%. The thermal conductivity of the GF is about 3

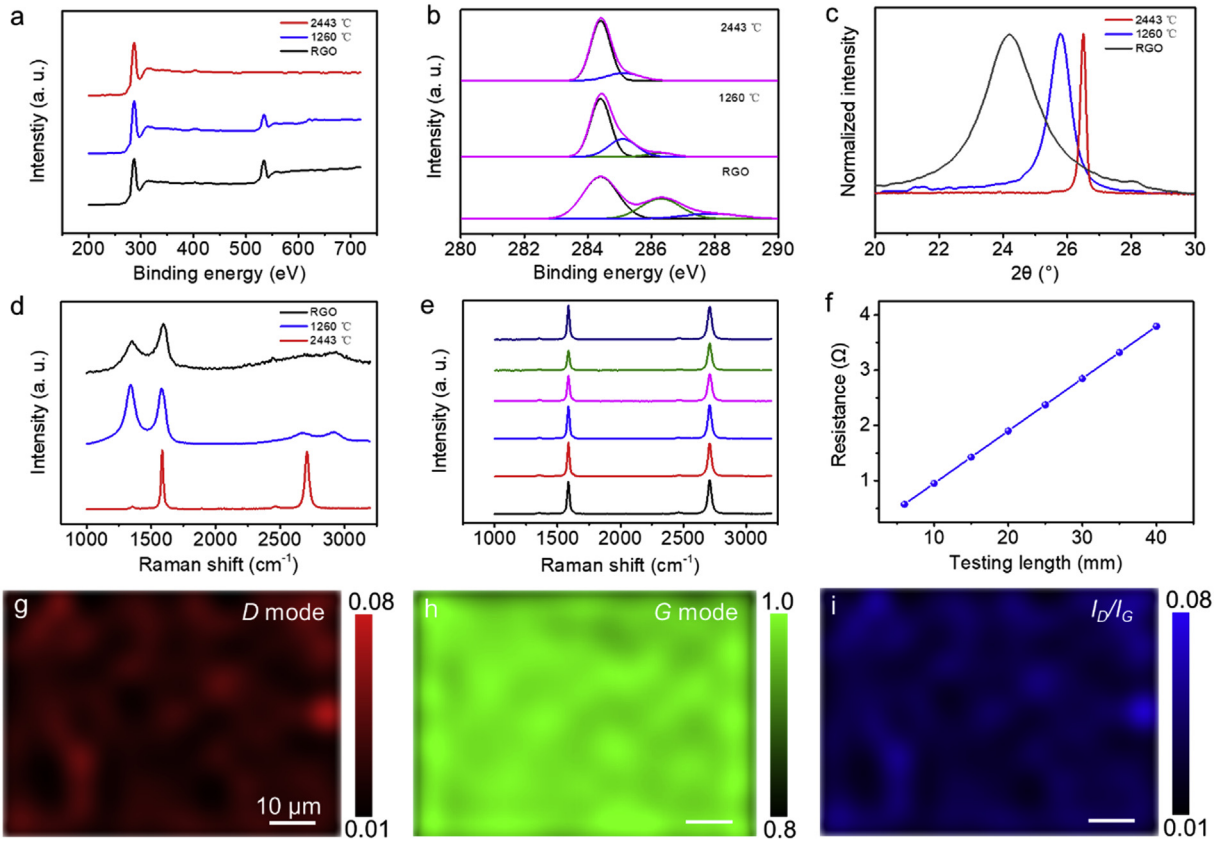

Fig. 3. (a-d) XPS spectra (a, b), XRD patterns (c), and Raman spectra (d) of rGO film before and after Joule heating at different temperatures. (e) Raman spectra collected at different sites of the Joule heated GF. The distance of each collecting site was about 1 cm. (f) Resistance of the sample as a function of testing length. (g-i) Raman mapping of D band (d), G band (e), and I_D/I_G (f) of the Joule heated GF at 2443 °C. (A colour version of this figure can be viewed online.)

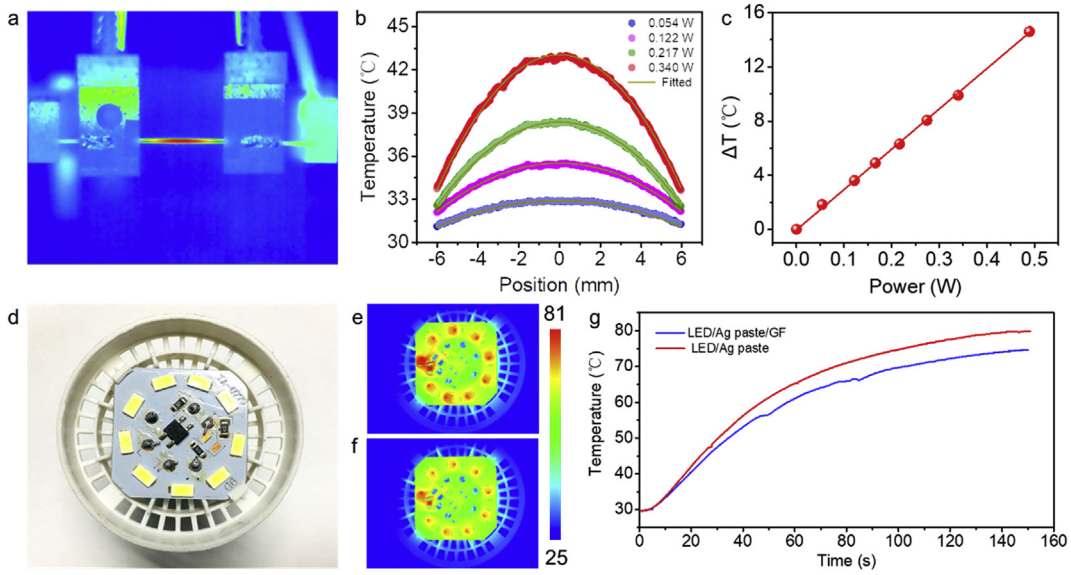

Fig. 4. (a) Infrared thermal image of a GF strip suspended on four copper electrodes. (b) Temperature profiles of Joule heated GF samples at different electrical power. (c) Temperature rise as a function of input power. (d) Photo of LED lamp. (e) Infrared thermal image of the LED lamp coated with Ag paste at working state. (f) Infrared thermal image of the LED lamp integrated with GF and Ag paste at the back side. (g) Real-time temperature mnoitoring curves of the LED with and without GF. (A colour version of this figure can be viewed online.)

times as high as that of pure copper (400 W/mK), 6 times as high as that of the best magnetically aligned discrete CNT films (200 W/m) [42], about 68% higher than that of aligned carbon nanotubes (CNTs) papers with high density (≈766 W/mK) [43], and comparable to that of GF (800–1500 W/mK) assembled from exfoliated graphene nanoplatelets with further annealing in furnace

[15,18,34,44]. The electrical conductivity of GF was calculated to be 4.2×10^5 S/m, 10 times higher than that of rGO film. Such enhancement in thermal/electrical conductivity of our GF can be attributed to the highly crystalline graphene structure and reduced phonon-boundary scattering resulting from the synergistic effect of high temperature Joule annealing and mechanical compaction by graphite rollers.

To evaluate the thermal management performance, the GF was pasted on the back side of a 5 W LED lamp by silver glue (Fig. 4d). According to the infrared thermal images, the highest temperature of the LED incorporated with GF/Ag paste is ~74 °C (Fig. 4f), about 6 °C lower than that of silver pasted LED (~80 °C, Fig. 4e). We monitored the real-time temperature changes of the LED (Fig. 4g). Both the temperature rising rate and the steady temperature of the LED/Ag paste/GF was lower than that of LED/Ag paste, demonstrating that the GF can be used as a promising thermal dissipation material for electronics. Additionally, we briefly compared the thermal conductivity, reduction time and production cost of various GFs reported thus far. Chemical reduction usually takes more than 10 h to get a moderate conductivity of 100–500 W/mK [16,45]. The production cost of thermally conductive film is mainly concentrated on the electric power consumption during carbonization/graphitization process. Conventional thermal annealing in electrical furnace can attain GF with higher thermal conductivity, but it needs much longer time (at least two days) and huge energy cost due to the slow heating and cooling rates. The average electric power per hour of the mini high-temperature graphitization furnace is about 50–70 kW/h and the total heating time is about 6–10 h. On the contrary, our roll-to-roll based Joule heating reduction method can be completed within tens of minutes with high energy efficiency. The total electrical power consumption for a thin film in this work is less than 3 KW. Obviously, the intensive Joule heating in a roll-to-roll manner is more time-saving, energy-efficient, and cost-effective, especially for the experimental prototype production. Considering the combined merits of ultrafast manufacturing process and satisfied thermal conductivity of the as-prepared GF, this facile roll-to-roll approach should have great potential to replace the traditional energy/time-consuming heating method by electrical furnace.

4. Conclusions

In this work, we report a rapid approach to fabricate continuous GF by Joule heating of rGO film integrated with a high-throughput roll-to-roll process. The achieved GF demonstrates superior flexibility and excellent electrical and thermal properties with the electrical conductivity of 4.2×10^5 S/m and thermal conductivity of 1285 ± 20 W/mK. When compared with traditional reduction method by electrical furnace, the intensive Joule heating in a roll-to-roll manner is more time-saving, energy-efficient, and cost-effective. Such facial processing strategy will enable the scaled-up manufacturing of large area and flexible GF with potential applications in thermal management, energy batteries, and wearable electronics.

Acknowledgements

The authors thank the staffs of the SSRF for SAXS characterizations. This work is supported by the National Natural Science Foundation of China (Nos. 51803177, 51533008, 21325417, 51703194, 51603183), National Key R&D Program of China (No. 2016YFA0200200), Fundamental Research Funds for the Central Universities (Nos. 2017QNA4036), Hundred Talents Program of Zhejiang University (188020*194231701/113), the key research and development plan of Zhejiang Province (2018C01049), the China Postdoctoral Science Foundation (Nos. 2017M620241), and the National Postdoctoral Program for Innovative Talents (No. BX201700209).

Appendix A. Supplementary data

Supplementary data to this article can be found online at https://doi.org/10.1016/j.carbon.2019.09.021.

References

[1] R. Ma, Z. Zhang, K. Tong, D. Huber, R. Kornbluh, Y.S. Ju, Q. Pei, Highly efficient electrocaloric cooling with electrostatic actuation, Science 357 (2017) 1130–1134.
[2] A.A. Balandin, Chill out, IEEE Spectrum 46 (2009) 34–39.
[3] R. Mahajan, C.-p. Chiu, G. Chrysler, Cooling a microprocessor chip, Proc. IEEE 94 (2006) 1476–1486.
[4] A. Majumdar, Thermoelectric devices: helping chips to keep their cool, Nat. Nanotechnol. 4 (2009) 214–215.
[5] R. Prasher, Graphene spreads the heat, Science 328 (2010) 185–186.
[6] M. Inagaki, L.-J. Meng, T. Ibuki, M. Sakai, Y. Hishiyama, Carbonization and graphitization of polyimide film "Novax", Carbon 29 (1991) 1239–1243.
[7] M. Inagaki, S. Harada, T. Sato, T. Nakajima, Y. Horino, K. Morita, Carbonization of polyimide film "Kapton", Carbon 27 (1989) 253–257.
[8] Y. Suhng, K. Hashizume, T. Kaneko, S. Otani, S. Yoshimura, The study of the graphitization behavior for polyimide and polyamide films, Synth. Met. 71 (1995) 1751–1752.
[9] A.A. Balandin, S. Ghosh, W. Bao, I. Calizo, D. Teweldebrhan, F. Miao, C.N. Lau, Superior thermal conductivity of single-layer graphene, Nano Lett. 8 (2008) 902–907.
[10] A.A. Balandin, Thermal properties of graphene and nanostructured carbon materials, Nat. Mater. 10 (2011) 569–581.
[11] S. Chen, Q. Wu, C. Mishra, J. Kang, H. Zhang, K. Cho, W. Cai, A.A. Balandin, R.S. Ruoff, Thermal conductivity of isotopically modified graphene, Nat. Mater. 11 (2012) 203–207.
[12] W. Lee, K.D. Kihm, H.G. Kim, S. Shin, C. Lee, J.S. Park, S. Cheon, O.M. Kwon, G. Lim, W. Lee, In-plane thermal conductivity of polycrystalline chemical vapor deposition graphene with controlled grain sizes, Nano Lett. 17 (2017) 2361–2366.
[13] K.M. Shahil, A.A. Balandin, Graphene–multilayer graphene nanocomposites as highly efficient thermal interface materials, Nano Lett. 12 (2012) 861–867.
[14] J.H. Seol, I. Jo, A.L. Moore, L. Lindsay, Z.H. Aitken, M.T. Pettes, X. Li, Z. Yao, R. Huang, D. Broido, N. Mingo, R.S. Ruoff, L. Shi, Two-dimensional phonon transport in supported graphene, Science 328 (2010) 213–216.
[15] G. Xin, H. Sun, T. Hu, H.R. Fard, X. Sun, N. Koratkar, T. Borca-Tasciuc, J. Lian, Large-area freestanding graphene paper for superior thermal management, Adv. Mater. 26 (2014) 4521–4526.
[16] W. Nan, M.K. Samani, H. Li, L. Dong, Z. Zhang, P. Su, S. Chen, J. Chen, S. Huang, G. Yuan, X. Xu, B. Li, K. Leifer, L. Ye, J. Liu, Large-area free-standing and ultrathin graphene films with superior thermal conductivity, Small 14 (2018) 1801346.
[17] L. Peng, Z. Xu, Z. Liu, Y. Guo, P. Li, C. Gao, Ultrahigh thermal conductive yet superflexible graphene films, Adv. Mater. 29 (2017) 1700589.
[18] C. Teng, D. Xie, J. Wang, Z. Yang, G. Ren, Y. Zhu, Ultrahigh conductive graphene paper based on ball-milling exfoliated graphene, Adv. Funct. Mater. 27 (2017) 1700240.
[19] G. Xin, T. Yao, H. Sun, S.M. Scott, D. Shao, G. Wang, J. Lian, Highly thermally conductive and mechanically strong graphene fibers, Science 349 (2015) 1083–1087.
[20] Z. Xu, Y. Liu, X. Zhao, L. Peng, H. Sun, Y. Xu, X. Ren, C. Jin, P. Xu, M. Wang, C. Gao, Ultrastiff and strong graphene fibers via full-scale synergetic defect engineering, Adv. Mater. 28 (2016) 6449–6456.
[21] Y. Wang, Y. Chen, S.D. Lacey, L. Xu, H. Xie, T. Li, V.A. Danner, L. Hu, Reduced graphene oxide film with record-high conductivity and mobility, Mater. Today 21 (2018) 186–192.
[22] Y. Chen, K. Fu, S. Zhu, W. Luo, Y. Wang, Y. Li, E. Hitz, Y. Yao, J. Dai, J. Wan, V.A. Danner, T. Li, L. Hu, Reduced graphene oxide films with ultrahigh conductivity as Li-ion battery current collectors, Nano Lett. 16 (2016) 3616–3623.
[23] Y. Chen, Y. Li, Y. Wang, K. Fu, V.A. Danner, J. Dai, S.D. Lacey, Y. Yao, L. Hu, Rapid, in situ synthesis of high capacity battery anodes through high temperature radiation-based thermal shock, Nano Lett. 16 (2016) 5553–5558.
[24] T. Li, A.D. Pickel, Y. Yao, Y. Chen, Y. Zeng, S.D. Lacey, Y. Li, Y. Wang, J. Dai, Y. Wang, B. Yang, M.S. Fuhrer, A. Marconnet, C. Dames, D.H. Drew, L. Hu, Thermoelectric properties and performance of flexible reduced graphene oxide films up to 3,000 K, Nat. Energy 3 (2018) 148–156.
[25] Y. Yao, K.K. Fu, C. Yan, J. Dai, Y. Chen, Y. Wang, B. Zhang, E. Hitz, L. Hu, Three-dimensional printable high-temperature and high-rate heaters, ACS Nano 10 (2016) 5272–5279.
[26] Y. Yao, K.K. Fu, S. Zhu, J. Dai, Y. Wang, G. Pastel, Y. Chen, T. Li, C. Wang, T. Li, L. Hu, Carbon welding by ultrafast joule heating, Nano Lett. 16 (2016) 7282–7289.

[27] Y. Yao, Z. Huang, P. Xie, S.D. Lacey, R.J. Jacob, H. Xie, F. Chen, A. Nie, T. Pu, M. Rehwoldt, D. Yu, M.R. Zachariah, C. Wang, R. Shahbazian-Yassar, J. Li, L. Hu, Carbothermal shock synthesis of high-entropy-alloy nanoparticles, Science 359 (2018) 1489–1494.
[28] Y. Chen, Y. Wang, S. Zhu, K. Fu, X. Han, Y. Wang, B. Zhao, T. Li, B. Liu, Y. Li, J. Dai, H. Xie, T. Li, J.W. Connell, Y. Lin, L. Hu, Nanomanufacturing of graphene nanosheets through nano-hole opening and closing, Mater. Today 24 (2018) 26–32.
[29] W. Bao, A.D. Pickel, Q. Zhang, Y. Chen, Y. Yao, J. Wan, K. Fu, Y. Wang, J. Dai, H. Zhu, D. Drew, M. Fuhrer, C. Dames, L. Hu, Flexible, high temperature, planar lighting with large scale printable nanocarbon paper, Adv. Mater. 28 (2016) 4684–4691.
[30] D. Yu, L. Dai, Voltage-induced incandescent light emission from large-area graphene films, Appl. Phys. Lett. 96 (2010) 143107.
[31] Y.D. Kim, H. Kim, Y. Cho, J.H. Ryoo, C.-H. Park, P. Kim, Y.S. Kim, S. Lee, Y. Li, S.-N. Park, Y.S. Yoo, D. Yoon, V.E. Dorgan, E. Pop, T.F. Heinz, J. Hone, S.-H. Chun, H. Cheong, S.W. Lee, M.-H. Bae, Y.D. Park, Bright visible light emission from graphene, Nat. Nanotechnol. 10 (2015) 676–681.
[32] M. Freitag, H.-Y. Chiu, M. Steiner, V. Perebeinos, P. Avouris, Thermal infrared emission from biased graphene, Nat. Nanotechnol. 5 (2010) 497–501.
[33] Y. Chen, G.C. Egan, J. Wan, S. Zhu, R.J. Jacob, W. Zhou, J. Dai, Y. Wang, V.A. Danner, Y. Yao, K. Fu, Y. Wang, W. Bao, T. Li, M.R. Zachariah, L. Hu, Ultra-fast self-assembly and stabilization of reactive nanoparticles in reduced graphene oxide films, Nat. Commun. 7 (2016) 12332.
[34] B. Shen, W. Zhai, W. Zheng, Ultrathin flexible graphene film: an excellent thermal conducting material with efficient EMI shielding, Adv. Funct. Mater. 24 (2014) 4542–4548.
[35] C. Bommier, T.W. Surta, M. Dolgos, X. Ji, New mechanistic insights on Na-ion storage in nongraphitizable carbon, Nano Lett. 15 (2015) 5888–5892.
[36] Y. Liu, Z. Xu, J. Zhan, P. Li, C. Gao, Superb electrically conductive graphene fibers via doping strategy, Adv. Mater. 28 (2016) 7941–7947.
[37] G. Xin, W. Zhu, Y. Deng, J. Cheng, L.T. Zhang, A.J. Chung, S. De, J. Lian, Microfluidics-enabled orientation and microstructure control of macroscopic graphene fibres, Nat. Nanotechnol. 14 (2019) 168–175.
[38] M.A. Worsley, P.J. Pauzauskie, T.Y. Olson, J. Biener, J.H. Satcher Jr., T.F. Baumann, Synthesis of graphene aerogel with high electrical conductivity, J. Am. Chem. Soc. 132 (2010) 14067–14069.
[39] M.A. Worsley, T.T. Pham, A. Yan, S.J. Shin, J.R. Lee, M. Bagge-Hansen, W. Mickelson, A. Zettl, Synthesis and characterization of highly crystalline graphene aerogels, ACS Nano 8 (2014) 11013–11022.
[40] A.C. Ferrari, J. Meyer, V. Scardaci, C. Casiraghi, M. Lazzeri, F. Mauri, S. Piscanec, D. Jiang, K. Novoselov, S. Roth, A.K. Geim, Raman spectrum of graphene and graphene layers, Phys. Rev. Lett. 97 (2006) 187401.
[41] A.C. Ferrari, D.M. Basko, Raman spectroscopy as a versatile tool for studying the properties of graphene, Nat. Nanotechnol. 8 (2013) 235–246.
[42] J. Hone, M.C. Llaguno, N.M. Nemes, A.T. Johnson, J.E. Fischer, D.A. Walters, M.J. Casavant, J. Schmidt, R.E. Smalley, Electrical and thermal transport properties of magnetically aligned single wall carbon nanotube films, Appl. Phys. Lett. 77 (2000) 666–668.
[43] L. Zhang, G. Zhang, C. Liu, S. Fan, High-density carbon nanotube buckypapers with superior transport and mechanical properties, Nano Lett. 12 (2012) 4848–4852.
[44] Y. Huang, Q. Gong, Q. Zhang, Y. Shao, J. Wang, Y. Jiang, M. Zhao, D. Zhuang, J. Liang, Fabrication and molecular dynamics analyses of highly thermal conductive reduced graphene oxide films at ultra-high temperatures, Nanoscale 9 (2017) 2340–2347.
[45] M. Zhang, Y. Wang, L. Huang, Z. Xu, C. Li, G. Shi, Multifunctional pristine chemically modified graphene films as strong as stainless steel, Adv. Mater. 27 (2015) 6708–6713.